

March 1995

hep-ph/9502276, DUKE-TH-95-85  
JHU-TIPAC-950004, YCTP-P4-95, EFI-95-06

# Wavepacket Dynamics in Yang–Mills Theory

**C.R. Hu<sup>1</sup>, S.G. Matinyan<sup>2</sup>, B. Müller<sup>3</sup>, and A. Trayanov<sup>4</sup>**

*Department of Physics, Duke University, Durham NC 27708-0305*

**T.M. Gould<sup>5</sup>**

*Dept. of Physics and Astronomy, The Johns Hopkins University, Baltimore MD 21218*

**S.D.H. Hsu<sup>6</sup>**

*Sloane Physics Laboratory, Yale University, New Haven CT 06511*

**E.R. Poppitz<sup>7</sup>**

*The Enrico Fermi Institute, University of Chicago, Chicago IL 60637*

## Abstract

We discuss the results of numerical simulations of colliding wavepackets in  $SU(2)$  Yang–Mills theory. We investigate their behavior as a function of amplitude and momentum distribution. We find regions in our parameter space in which initial wave packets scatter into final configurations with dramatically different momentum distributions. These results constitute new classical trajectories with multiparticle boundary conditions. We explain their relevance for the calculation of scattering amplitudes in the semiclassical approximation. Finally, we give directions for future work.

---

<sup>1</sup>chaoran@phy.duke.edu

<sup>2</sup>On leave from Yerevan Physical Institute, Yerevan 375036, Armenia. E-mail: ani@phy.duke.edu

<sup>3</sup>muller@phy.duke.edu

<sup>4</sup>Permanent address: NCSC, Research Triangle Park, North Carolina 27708. E-mail: nasco@phy.duke.edu

<sup>5</sup>gould@fermi.pha.jhu.edu

<sup>6</sup>hsu@hsunext.physics.yale.edu

<sup>7</sup>epoppitz@yukawa.uchicago.edu

# 1 Introduction

Two recent observations on the dynamics of Yang–Mills theory can be combined to yield new nonperturbative information about scattering amplitudes in non-Abelian gauge theories. In [1], it was shown that the existence of real trajectories satisfying multiparticle boundary conditions implies high multiplicity scattering amplitudes which are not suppressed in the weak coupling limit. In [2], it was found that a standing plane wave is unstable in  $SU(2)$  Yang-Mills theory.

The authors of [1] developed a stationary phase approximation for computing scattering amplitudes. When the stationary trajectory is real, it satisfies an initial value problem, consisting of the classical field equations with wavepacket initial conditions, and describes a classically allowed transition<sup>1</sup>. In this case, there is no exponential suppression of the associated scattering amplitude at small coupling, as opposed to disallowed, or tunneling transitions. The first step in this program is to find such trajectories. The complicated nature of the field equations necessitates a computational approach.

Indeed, progress in this direction has already been made. In studying the chaotic dynamics of Yang–Mills theory, the authors of [2] have found evidence for an instability in the field equations which leads to a growth of long wavelength modes from initial short wavelength standing plane waves. The mechanism finds its origin in the non-Abelian spin-field coupling, which drives an instability for perturbations with isospin polarizations orthogonal to the standing plane wave [2].

This implies the existence of classical trajectories of the type required by [1], if the instability persists in the regime of localized wavepackets. One purpose of the present investigation is to determine the extent to which this is the case. The authors of [1] have already identified a mechanism which may produce interesting classical trajectories. Our goal in the current paper is to investigate this mechanism through numerical simulations on a lattice. For simplicity, we have studied wavepackets with constant profiles in the transverse directions.

Our interest in the problem addressed in this paper has its origin in the work of [3]. These authors suggested that multiparticle production could be unsuppressed in electroweak interactions at high energies and could manifest itself in fermion number violating processes. In order to investigate this phenomena further, previous authors have studied the classical analog of high energy particle collisions [4, 5]. The studies of one dimensional Abelian Higgs gauge theory [4] and  $\lambda\phi^4$  theory [5] have shown no indication for the classical analog of multiparticle scattering. The work of [1] establishes a precise connection between the classical results of [4, 5] and quantum scattering amplitudes.

This paper is organized as follows. In Section 2, we describe the numerical simulation. In Section 3, we discuss some of our results and their implications. In Section 4, we explain

---

<sup>1</sup>The general case of *complex* trajectories is discussed in [1].

the relevance of our computations to realistic three dimensional scattering. In Section 5, we summarize and give directions for future research.

## 2 Classical Yang–Mills Theory on the Lattice

In this section, we describe the numerical simulation [6]. For simplicity, we work with a one dimensional lattice with physical size  $L = Na$ , where  $N$  is the number of lattice sites and  $a$  the lattice spacing. We arrange initially two Gaussian wavepackets with average momenta  $(\bar{k}, 0, 0, \pm\bar{k})$ , and width  $\Delta k$ , between the maximum and minimum longitudinal momenta on the lattice  $k_{min}, k_{max}$ .

$$(k_{min} = 2\pi/Na) \ll \Delta k \ll \bar{k} \ll (k_{max} = 2\pi/2a) . \quad (2.1)$$

The packets are fairly narrow in momentum space,  $\Delta k/\bar{k} \ll 1$ .

The wavepackets are constant in the transverse  $x, y$  directions. Since, at time  $t = 0$ , the two wavepackets are arranged to be well-separated from each other and from the lattice boundaries, the gauge field  $A^{c,i}$  is initially

$$A^{c,i} = A_R^{c,i} + A_L^{c,i} . \quad (2.2)$$

We work in the  $A^0 = 0$  gauge,  $c$  is the isospin index,  $i$  the Lorentz index.  $A_R$  is a right-moving wavepacket, initially centered at  $z = Z_R$ .  $A_L$  is a left-moving wavepacket, initially centered at  $z = Z_L$ . In practice,  $Z_R$  and  $Z_L$  are chosen so that they are symmetrical about the center of the longitudinal lattice and  $\Delta Z \equiv Z_L - Z_R$  is large compared to  $1/\Delta k$ .

Both wavepackets are chosen to be polarized in the same spatial direction ( $i = 2$ ) for simplicity. Furthermore, the right-moving wavepacket is polarized in an isospin direction defined by a unit vector  $\hat{n}_R = (0, 0, 1)$

$$A_R^{c,i} = \delta^{i2} \hat{n}_R^c \phi(z - Z_R, -t) , \quad (2.3)$$

and the left-moving wavepacket is polarized in an isospin direction defined by another unit vector  $\hat{n}_L$

$$A_L^{c,i} = \delta^{i2} \hat{n}_L^c \phi(z - Z_L, t) . \quad (2.4)$$

Each wavepacket would therefore be stable in the absence of the other and would propagate as a collection of free travelling waves. The relative rotation between the two isospin vectors,  $\hat{n}_R \cdot \hat{n}_L \equiv \cos \theta_c$ , is a free parameter in our computation. Nonlinear terms in the Yang–Mills equations arise from commutators which vanish at  $\theta_c = 0$ .

The wavepacket is chosen as a Gaussian

$$\phi(z, t) = \sqrt{\frac{2 \Delta k}{\pi^{1/2} \sigma \bar{k}}} \exp\left(-\frac{1}{2}(\Delta k)^2 (z + t)^2\right) \cos\left(\bar{k}(z + t)\right) . \quad (2.5)$$

This expression comes from the Fourier transform of a Gaussian momentum space distribution, after dropping some exponentially small corrections  $\mathcal{O}(e^{-(\bar{k}/\Delta k)^2/2})$ . There is no intrinsic mass scale in classical Yang–Mills theory. So, dimensionful parameters will be determined by the lattice spacing  $a$ .

Our study is based on the Hamiltonian formulation of lattice  $SU(2)$  gauge theory [7], in which the dynamic variables are link variables defined as

$$U_l = \exp\left(-\frac{i}{2} g a A_l^a \tau^a\right). \quad (2.6)$$

where  $l$  stands for the link index and  $\tau^c$  ( $c = 1, 2, 3$ ) are Pauli matrices.

For  $z < L/2$ , the link variable is approximately that of the right–moving wavepacket:

$$U_l = \cos\left(\frac{1}{2} g a \phi(z - Z_R, -t)\right) + i \tau \cdot \hat{n}_R \sin\left(\frac{1}{2} g a \phi(z - Z_R, -t)\right) \quad \text{if } l = 2. \quad (2.7)$$

For  $z > L/2$ , the link variable is approximately that of the left–moving wavepacket:

$$U_l = \cos\left(\frac{1}{2} g a \phi(z - Z_L, t)\right) + i \tau \cdot \hat{n}_L \sin\left(\frac{1}{2} g a \phi(z - Z_L, t)\right) \quad \text{if } l = 2. \quad (2.8)$$

We are evolving wavepackets which are initially free, and therefore the initial value of  $\dot{U}_l$  is just the time derivative of  $U_l$  as given in (2.7) and (2.8).

Our ansatz for the initial wavepackets has four free parameters. The relative isospin polarizations of the two packets is parametrized by  $\theta_c$ . There are two free momentum scales: the average momentum of the wavepackets  $\bar{k}$  and their width  $\Delta k$ . Finally, the amplitude is controlled by the free parameter  $\sigma$ . The coupling  $g$  can be rewritten in terms of the parameter  $\sigma$  by rescaling the field in the equations and initial conditions. To see this explicitly, let  $A' = \sqrt{\sigma} A$  and  $F'^{\mu\nu} = \sqrt{\sigma} F^{\mu\nu} = \partial^\mu A'^\nu - \partial^\nu A'^\mu + ig'[A'^\mu, A'^\nu]$ , where  $g' = g/\sqrt{\sigma}$ . Then, with respect to the scaled gauge potential  $A'^\mu$ , the equation of motion reads

$$\partial_\mu F'^{\mu\nu} + ig' [A'_\mu, F'^{\mu\nu}] = 0. \quad (2.9)$$

Since  $A'^\mu$  is only dynamically dependent on the coupling  $g'$ , we conclude that the system shows the same dynamics for different values of  $g$  and  $\sigma$ , as long as the ratio  $g' = g/\sqrt{\sigma}$  is held fixed.

In the next section, we describe the behavior of our simulations with respect to the parameters mentioned above (we fix the coupling  $g = 1$ ).

## 3 Results from Colliding Wavepackets

### 3.1 Snapshots

First, we present two figures of the field amplitude itself to illustrate some collisions qualitatively, plotting successive time slices of the norm of the field. Figure 1 shows an elastic collision of wavepackets with no relative isospin polarization. The wavepackets pass through each other without interacting, as expected. This constitutes a check on our numerical procedure and shows the nonlinearities introduced by the formulation in terms of compact lattice gauge fields do not affect the scattering process.

Figure 2 illustrates an inelastic collision of wavepackets with maximal (orthogonal) relative isospin polarization, for the same values of  $\bar{k}$  and  $\Delta k$ . The wavepackets are distorted after the collision and clearly contain modes in a range around the initial momentum distribution. As we will discuss below, inelastic collisions remain qualitatively similar for relative polarizations as small as  $\mathcal{O}(10^{-12})$ , all other parameters held fixed. In the following two subsections, we specialize to the case of *orthogonal* isospin polarization.

It should be noted that the fields do not linearize at late times in our simulation. In the absence of dispersion, the energy density of each packet is always bounded in time in one dimensional collisions, and the fields are not expected to linearize at large times. As a result, quantities like energy spectra do not settle down to constants at late times. One consequence for us is that it will not make sense to infer any characteristics about a “final” state from the late time behavior on our lattice. In the full three dimensional situation, geometry allows energy densities to spread out in space and to approach the linear regime. In this case, we expect to see the spectrum approach a constant at late times. Lacking this time scale in our one dimensional simulation, we simply allow our simulation to run as long as it would take two non-interacting wavepackets to pass through each other and become well-separated,  $t \simeq 600$ , see Figure 1. The relevance of our one dimensional simulations for the three dimensional physics will be discussed further in section 4.

### 3.2 Energy spectrum

To illustrate the broadening of momentum distribution after collision, Figures 3 and 4, in correspondence with Figures 1 and 2 respectively, show the time evolution of the absolute value of the Fourier transform of the energy density

$$\mathcal{E}(\mathbf{k}, t) = \frac{1}{4} \left| \int d^3x e^{i\mathbf{k}\cdot\mathbf{x}} \text{Tr} \left[ \mathbf{E}^2(\mathbf{x}, t) + \mathbf{B}^2(\mathbf{x}, t) \right] \right|, \quad (3.1)$$

where  $\mathbf{E}$  is the isospin electric field and  $\mathbf{B}$  the isospin magnetic field. As expected, the spectrum for parallel polarization (Figure 3) remains unchanged in the time allowed by the simulation, with a peak at roughly twice the average momentum  $\bar{k}$ . The spectrum for orthogonal polarization (Figure 4) is strongly disrupted due to nonlinear interactions. In each of these figures, the spike at  $k = 0$  is the total energy of the wavepackets, and its constancy provides a check on our computation.

### 3.3 Amplitude and width dependence

By rescaling coordinates, the initial configuration (2.5) can be rewritten

$$\phi'(z', t') \equiv \phi(z, t)/\bar{k} = \sqrt{\frac{2R}{\pi^{1/2}}} \exp\left(- (z' + t')^2 / 2W^2\right) \cos(z' + t') , \quad (3.2)$$

in terms of dimensionless spacetime coordinates,  $z' \equiv \bar{k}z$  and  $t' \equiv \bar{k}t$ , and dimensionless parameters,  $R \equiv \Delta k / \sigma \bar{k}^3$  and  $W \equiv \bar{k} / \Delta k$ . We refer to  $R$  as the amplitude parameter and  $W$  as the width parameter. The initial separation between the wavepackets in dimensionless units is  $\bar{k}\Delta Z$ . Thus, the time evolution of configurations with the same dimensionless parameters are identical in the *continuum*.

However, the lattice simulation necessarily involves two more dimensional parameters: the length  $L$  of the lattice and the lattice spacing  $a$ . We have chosen both  $L$  and also  $\Delta Z$  large enough compared to the width of the wavepacket that their effects can be neglected. The scaled lattice spacing  $a' = \bar{k}a$  is the number of lattice points representing a single wavelength, and specifies how close the simulation is to the continuum limit. We have checked that the qualitative behavior of our simulation is not sensitive to the choice of  $a'$ . Therefore, we present our results with fixed lattice spacing  $a = 1$  and  $\bar{k} = \pi/10$ . (This corresponds to 20 lattice points in a single wavelength). The scaling property explicit in (3.2) provides a check that our lattice is close to the continuum limit. Simulations with the same dimensionless parameters,  $R$  and  $W$ , should be identical. We have verified that our results are consistent with this scaling.

Figure 5 displays the dependence of the energy spectrum on the initial dimensionless amplitude  $R$ , with the width parameter  $W$  fixed. The nonlinearity clearly gets weaker as the amplitude  $R$  is decreased. Larger values of  $\sigma$  require longer times for the development of comparable nonlinearities. This is analogous to the case of the standing wave configuration where the largest Lyapunov exponent is a linear function of the amplitude [2].

Figures 6 and 7 display the dependence of the energy spectrum on the width parameter  $W$ , with  $R$  fixed. In the figures,  $W$  varies by a factor of 5. We expect that wider packets overlap for longer times during collision and should behave more nonlinearly. We see that the instability is always more pronounced in the widest packet ( $W = 25$ ) versus the narrowest ( $W = 5$ ). However, lacking a quantitative measure of nonlinearity it is hard to characterize exactly what is happening when we compare other values of  $W$ .

### 3.4 Dependence on isospin polarization

We now consider the dependence on the initial isospin polarization of the wavepackets. As given in Section 2, the right-moving packet is initially polarized in the isospin  $c = 3$  direction, while the left-moving packet is polarized in the isospin  $c = 2, 3$  plane. The relative angle  $\theta_c$  is varied from 0 to  $\pi$ .

Figure 8 shows the spectra at  $t = 600$  for different polarizations. Figure 9 shows the evolution of energy contained in the isospin  $c = 1$  component, modes orthogonal to both

initial packets. An exponential increase is seen for time  $t \approx 200$  or later in Figure 9. The largest overlap between the two wavepackets occurs at time  $t \approx 200$  when the centers of the two wavepackets meet. However, the energy drops after an exponential growth. Again, it does not approach a constant at late times after the collision due to the absence of dispersion in the one dimensional simulation.

It is remarkable that the nonlinear behavior persists until very small relative polarizations, near  $\theta_c = 10^{-12}\pi$ , where one might expect nonlinear effects to be perturbatively small. This was the case in the limit of large  $\sigma$ , where nonlinear effects disappeared entirely for  $\sigma$  as small as  $\mathcal{O}(10)$  (see Figure 5). However, the dynamics respond quite differently in the two limits. For large  $\sigma$ , the initial amplitude is small,  $\mathcal{O}(\sigma^{-1/2})$ , and all nonlinear terms in the field equations are suppressed. For small  $\theta_c$  however, the initial amplitude is not suppressed,  $\mathcal{O}(\theta_c^0)$ , and can drive instabilities.

Recall the initial gauge potential (2.2) has the form

$$\begin{aligned} A^i(t, \vec{x}) &= \delta^{i2} (\phi_R + \phi_L \cos \theta_c) \tau^3 + \delta^{i2} \phi_L \sin \theta_c \tau^2, \\ &= \delta^{i2} (\phi_R + \phi_L) \tau^3 + \delta^{i2} \phi_L \theta_c \tau^2 + \mathcal{O}(\theta_c^2). \end{aligned} \quad (3.3)$$

It evolves at some short time  $t$  later to the more general form

$$A^i(t, \vec{x}) = \delta^{i2} (\phi_R + \phi_L) \tau^3 + \delta^{i2} \phi_L \theta_c \tau^2 + b_i^a \tau^a + \mathcal{O}(\theta_c^2), \quad (3.4)$$

where  $b_i^a$  are small perturbations and may have any polarizations. The background field (3.3) driving this perturbation is not dissimilar from that studied in [2]. In the limit  $\theta_c \approx 0$ , it is a momentum superposition of isospin-polarized standing waves, which is unstable to small isospin-orthogonal perturbations, just as a single polarized standing wave is [2]. The Yang-Mills equations for (3.4) then imply equations for the perturbation of the form

$$\partial^\mu \partial_{[\mu} b_{\nu]} + \mathcal{O}(b \cdot (\phi_R + \phi_L)) + \mathcal{O}(b^2) + \mathcal{O}(\theta_c) = 0. \quad (3.5)$$

in which the coupling of the perturbation to the background is  $\mathcal{O}(\theta_c^0)$ . This coupling drives the instability (at least initially) with a growth rate determined by the associated largest Lyapunov exponent [2]. Thus, one understands why the instability persists even for very small relative polarizations, as seen in Figure 8. As a further check on our understanding of this limit, the cases with very small  $\theta_c$  in Figures 8 and 9 display the similar exponential growth found in [2].

## 4 Implications for three dimensions

In this section we discuss the implications of our one dimensional simulation for the behavior of wavepackets in three dimensions. Obviously, our simulation applies directly to three

dimensional configurations which are translationally invariant in the  $x - y$  plane. However, any configuration of this type must contain an infinite number of particles if the gauge field has nonzero amplitude.

Our simulation also applies to initial wavepackets with finite but large  $x - y$  extent. As sketched in Figure 10, the evolution of the core region  $x, y \approx 0$  is represented by the dotted part until time  $t \approx r_\perp$  in the world plane, while the evolution of the edge effect is bounded by two solid lines starting at  $r = r_\perp$  and  $t = 0$ . Clearly, if the transverse extent of the wavepackets  $r_\perp$  is larger than the total elapsed time of the simulation,

$$r_\perp > T_s , \tag{4.1}$$

then causality guarantees that the three dimensional evolution in the core region will be the same as that found in our simulation. Of course, we cannot deduce from our simulation what the final three dimensional configuration will be. However, we can at least conclude that some nonlinear activity, such as the redistribution of energy in momentum space, has occurred.

Thus our numerical results are predictive of the behavior of three dimensional wavepackets with pancake-like geometry (see Figure 11). This is precisely the geometry that one would expect for an initially roughly spherical wavepacket which has been boosted relative to the lab frame. For such wavepackets we can relate the parameters describing our initial configurations to the particle number of corresponding three dimensional wavepackets. Our choice of normalization in (2.5) is such that there is one particle per cross sectional area  $\sigma$ . This implies total particle number

$$N = \pi r_\perp^2 / \sigma , \tag{4.2}$$

where  $r_\perp$  must satisfy the inequality (4.1).

As an application of the above analysis, consider the simulation depicted in Figure 2. We see well developed effects of the nonlinear interactions by time  $t = 600$ . This implies that a three dimensional wavepacket of extent  $r_\perp > 600$ , which initially consists of  $N = \pi r_\perp^2 / \sigma$  particles, will exhibit interesting nonlinear interactions.

Of course, the extrapolation given above to three dimensions is somewhat conservative, relying only on causality. One might guess that for an initial wavepacket of the type depicted in Figure 11, in which the transverse momenta of individual modes is much smaller than their longitudinal momenta  $k_\perp \ll k_\parallel$ , the nonlinearities can continue to develop even at times after  $t = r_\perp$ . Individual modes will not disperse appreciably in the transverse direction until a time

$$t_d \approx \frac{k_\parallel}{k_\perp} r_\perp . \tag{4.3}$$

If this is the case, we should allow ourselves to follow the one dimensional simulations until time  $t_d$ , and conclude that the corresponding three dimensional simulation will behave



similarly. Since  $r_{\perp}$  can now be significantly smaller than the run time of the simulation, we would predict interesting nonlinear behavior for three dimensional wavepackets consisting of fewer particles than estimated above.

## 5 Conclusions

In this paper, we have described the behavior of one dimensional wavepacket collisions in pure Yang–Mills theory. We have seen evidence for the production of final states with dramatically different momentum distributions, but for initial states with large average multiplicity. When combined with the results of [1], these classical trajectories imply unsuppressed quantum scattering amplitudes in Yang–Mills theory, with initial wavepacket quantum states scattering to final states of very different multiplicity. It is worth recalling the situation which was found in the study of multiparticle electroweak processes including those with  $(B + L)$  violation. Certain processes with many particles (bosons) both in the initial and in the final state (*many*  $\rightarrow$  *many* scattering) can be shown to be unsuppressed within the semiclassical approximation [8]. The methods of [8] are Euclidean, and hence describe classically disallowed transitions, with the suppression disappearing as the energy approaches the barrier where the transitions are classically allowed. Because our simulations are in Minkowski space, they describe classically allowed processes.

Our simulations were performed with the coupling  $g = 1$ . By scaling the gauge potential, one can reach other values. For instance, Figure 2 implies nonlinear behavior for  $g = 1$ ,  $\sigma = 1$ , and initial state with  $N \approx 10^6$  particles (see (4.2)). Conversely a *two* particle collision, implying  $\tilde{\sigma} \approx 10^6$  on a one dimensional lattice of the same size, would require a coupling of  $\tilde{g} = g\sqrt{\tilde{\sigma}}/\sqrt{\sigma} \approx 10^3$  to exhibit similar nonlinear behavior (see (2.9)). For such a large value of the coupling constant, the semiclassical approximation would not be expected to be a good guide for the behavior of the quantum theory. In the language of [1], there is no window in values of the coupling constant which yields both interesting trajectories and controlled semiclassical corrections if we apply our conservative criterion (4.1) for applicability to three dimensions.

It is important to remember that the failure to find a trajectory connecting a two particle initial state and a many particle final state *does not* constitute conclusive evidence that  $2 \rightarrow$  *many* amplitudes are suppressed. Real Minkowski trajectories comprise only a subset of the complex trajectories which may dominate multiparticle scattering amplitudes at weak coupling [1].

There are a few immediate directions for improving our results.

1. We can refine our study by including transverse sites on the lattice. An asymmetric lattice may allow this improvement without drastically increasing the computation time. As mentioned in Section 4, this would allow us to study wavepackets with smaller transverse extent and fewer number of particles. We expect the one dimensional simulation to have

determined an upper bound on the critical number of particles in the three dimensional world, so that we anticipate finding nonlinear effects for smaller numbers of particles on the three dimensional lattice.

**2.** We can address the problem of multiparticle amplitudes in the electroweak theory by including a Higgs scalar. In this case, the explicit mass scale could act as a cut-off on long wavelength excitations. The additional possibilities of scalar-vector and scalar-scalar scattering add to the complexity of the parameter space.

These issues will be investigated in future research.

The authors would like to thank Krishna Rajagopal for useful comments on the scaling behavior of our results. This work was supported in part by the U.S. Department of Energy (Grant No. DE-FG05-90ER40592) at Duke University and by a computing grant from North Carolina Supercomputing Center. S.G.M. would specially like to thank Professor Vartan Gregorian, President of Brown University, and Office of International Programs of Duke University for their support. T.M.G. acknowledges the support of NSF grants NSF-PHY-90-96198 and NSF-PHY-94-04057. S.D.H.H. acknowledges the support of DOE contract DE-AC02-ERU3075 at Yale University. E.R.P. is supported by a Robert R. McCormick fellowship and by DOE contract DE-FGP2-90ER40560.

## References

- [1] T.M. Gould, S.D.H. Hsu, and E.R. Poppitz, *Nucl. Phys.* **B437**, 83 (1995).
- [2] C. Gong, S.G. Matinyan, B. Müller and A. Trayanov, *Phys. Rev.* **D49**, 607 (1994).
- [3] A. Ringwald, *Nucl. Phys.* **B330**, 1 (1990);  
O. Espinosa, *Nucl. Phys.* **B343**, 310 (1990);
- [4] K. Rajagopal and N. Turok, *Nucl. Phys.* **B375**, 299 (1992).
- [5] H. Goldberg, D. Nash and M.T. Vaughn, *Phys. Rev.* **D46**, 2585 (1992).
- [6] For additional details, see C. Gong, Duke University thesis.
- [7] J. Kogut and L. Susskind, *Phys. Rev.* **D11** 395 (1975);  
S.A. Chin, O.S. Van Roosmalen, E.A. Umland, and S.E. Koonin, *Phys. Rev.* **D31** 3201 (1985).
- [8] S. Yu Khlebnikov, V.A. Rubakov and P. G. Tinyakov, *Nucl. Phys.* **B367**, 334 (1991)

## Figures

Figure 1: Collision for parallel isospin polarization.  $\bar{k} = \pi/10$ ,  $\Delta k = \pi/100$ , and  $\sigma = 1$ . The wavepackets are initially separated by  $\Delta Z = 384$  on a lattice of length  $L = 1024$  and lattice spacing  $a = 1$ .

Figure 2: Same as Figure 1, but with orthogonal isospin polarization.

Figure 3: Time slices of energy spectrum (parallel isospin polarization).  $\bar{k} = \pi/10$ ,  $\Delta k = \pi/100$ , and  $\sigma = 1$ . The units for the momentum are  $\pi/512$ . The wavepackets are initially separated by  $\Delta Z = 384$  on a lattice of length  $L = 1024$  and lattice spacing  $a = 1$ .

Figure 4: Same as Figure 3, but with orthogonal isospin polarization.

Figure 5: Amplitude dependence of instability shown in terms of different  $\sigma$  at time  $t = 1200$  (orthogonal isospin polarization). Again we choose  $\bar{k} = \pi/10$  and  $\Delta k = \pi/100$ . This fixes the width parameter  $W = 10$ . Different values for the amplitude parameter  $R$  are obtained by varying  $\sigma$ . The units for the momentum are  $\pi/1024$ . The wavepackets are initially separated by  $\Delta Z = 1024$  on a lattice of length  $L = 2048$  and lattice spacing  $a = 1$ .

Figure 6: Fixed time slices of energy spectrum which show dependence of the instability on the dimensionless width of the wavepacket  $W$  with dimensionless amplitude  $R$  fixed. All time slices are at  $t = 800$  with  $\bar{k} = \pi/10$ ,  $a = 1$ ,  $L = 2048$  and  $\Delta Z = 1024$ . The units for the momentum are  $\pi/1024$ .

Figure 7: Same as Figure 6, but with  $t = 1200$ .

Figure 8: Spectra at  $t = 600$  for different isospin polarization  $\theta_c$ .  $\bar{k} = \pi/10$ ,  $\Delta k = \pi/100$ , and  $\sigma = 1$ . The units for the momentum are  $\pi/512$ . The wavepackets are initially separated by  $\Delta Z = 384$  on a lattice of length  $L = 1024$  and lattice spacing  $a = 1$ .

Figure 9: Energy contained in the isospin  $c = 1$  component of the gauge field, shown as a function of time in terms of different  $\theta_c$ .  $\bar{k} = \pi/10$ ,  $\Delta k = \pi/100$ , and  $\sigma = 1$ . The wavepackets are initially separated by  $\Delta Z = 384$  on a lattice of length  $L = 1024$  and lattice spacing  $a = 1$ .

Figure 10: The edge of the wavepacket at  $r_\perp$  is out of causal contact with the interior region for sufficiently short times  $t$ .

Figure 11: Collision of two wavepackets in coordinate space.

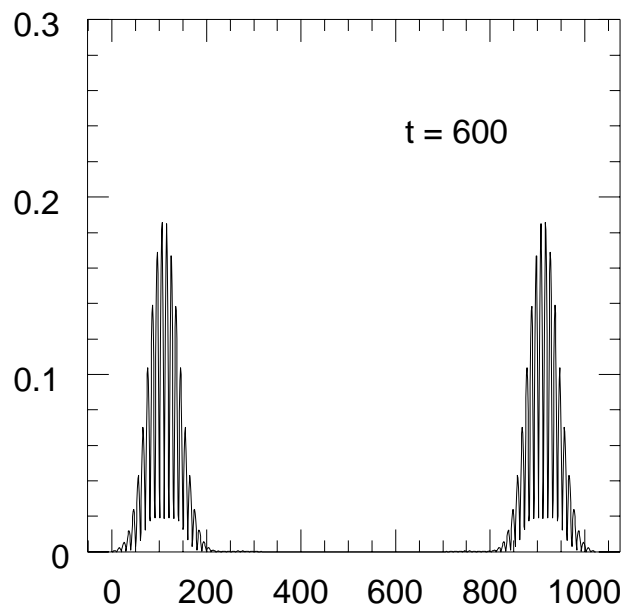
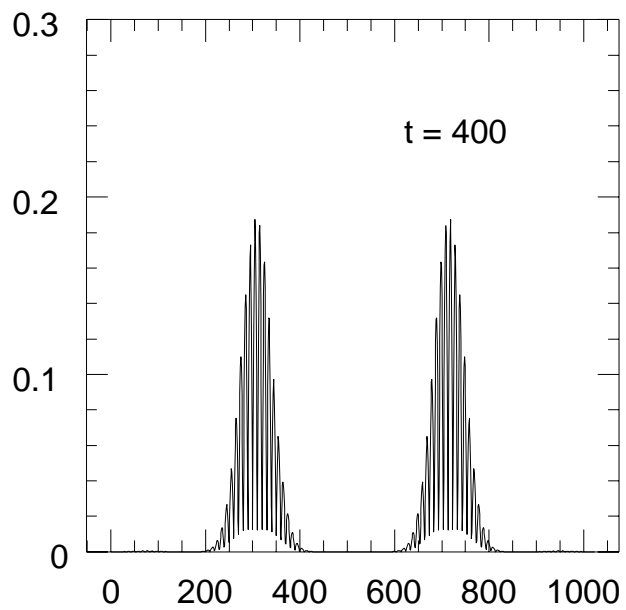
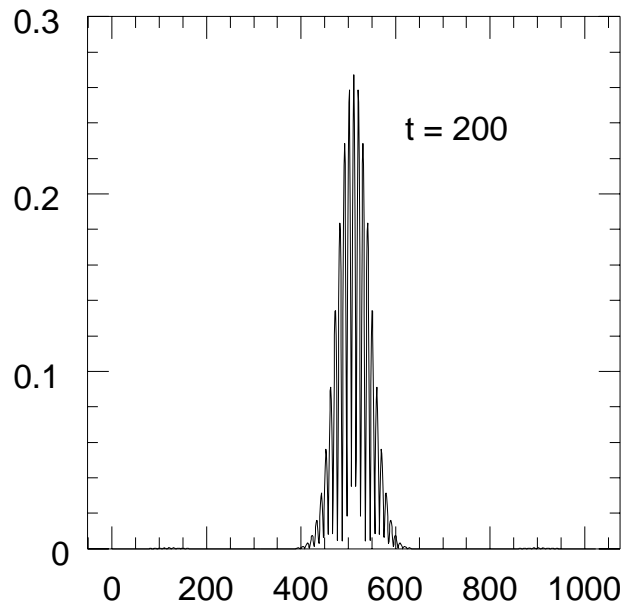
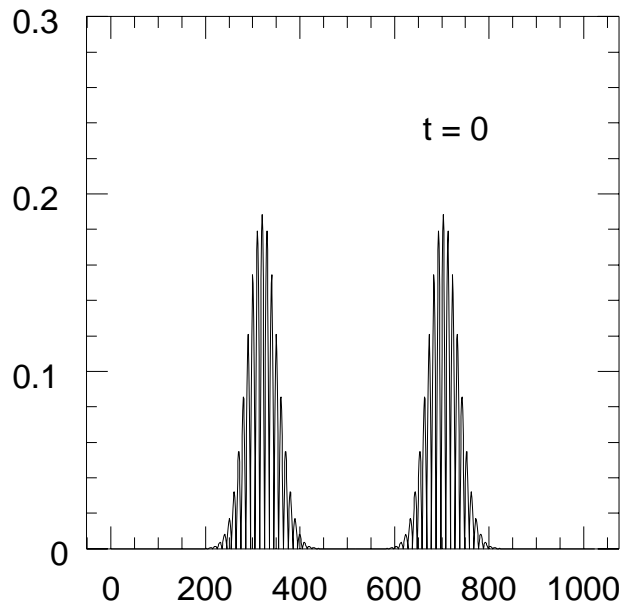


Fig.1

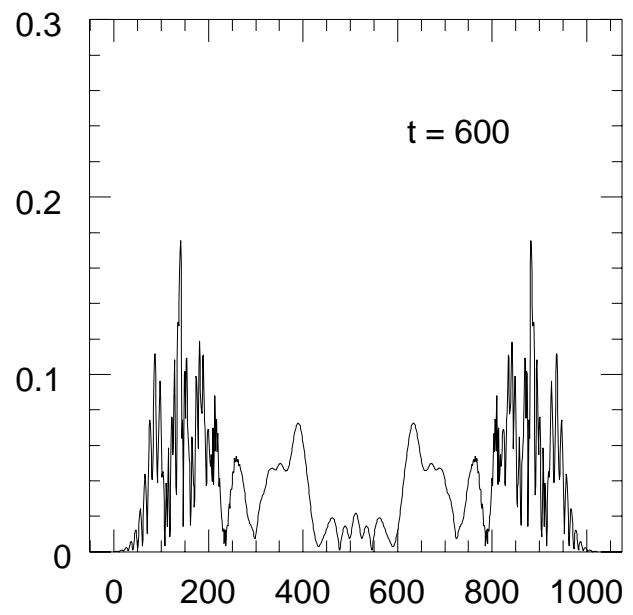
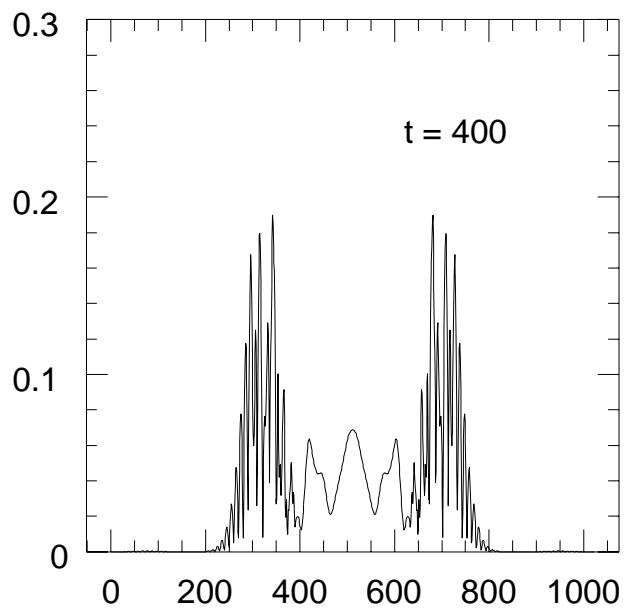
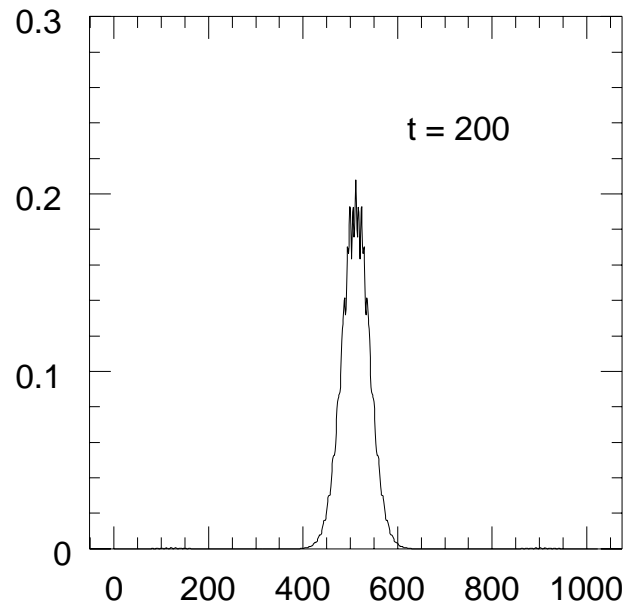
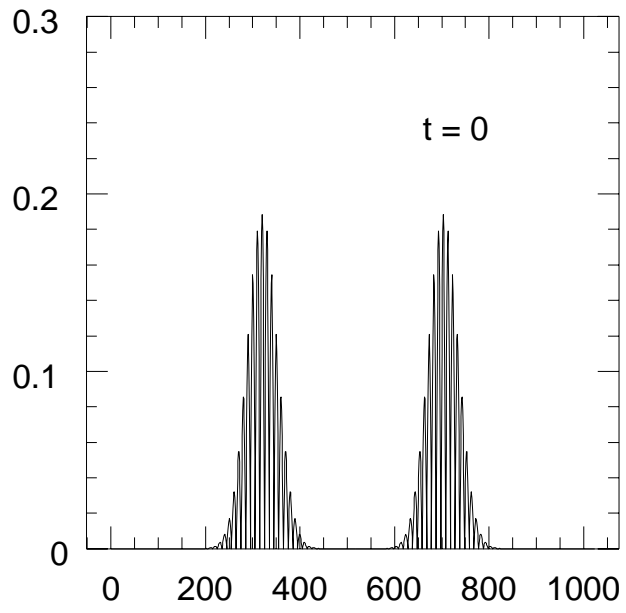


Fig.2

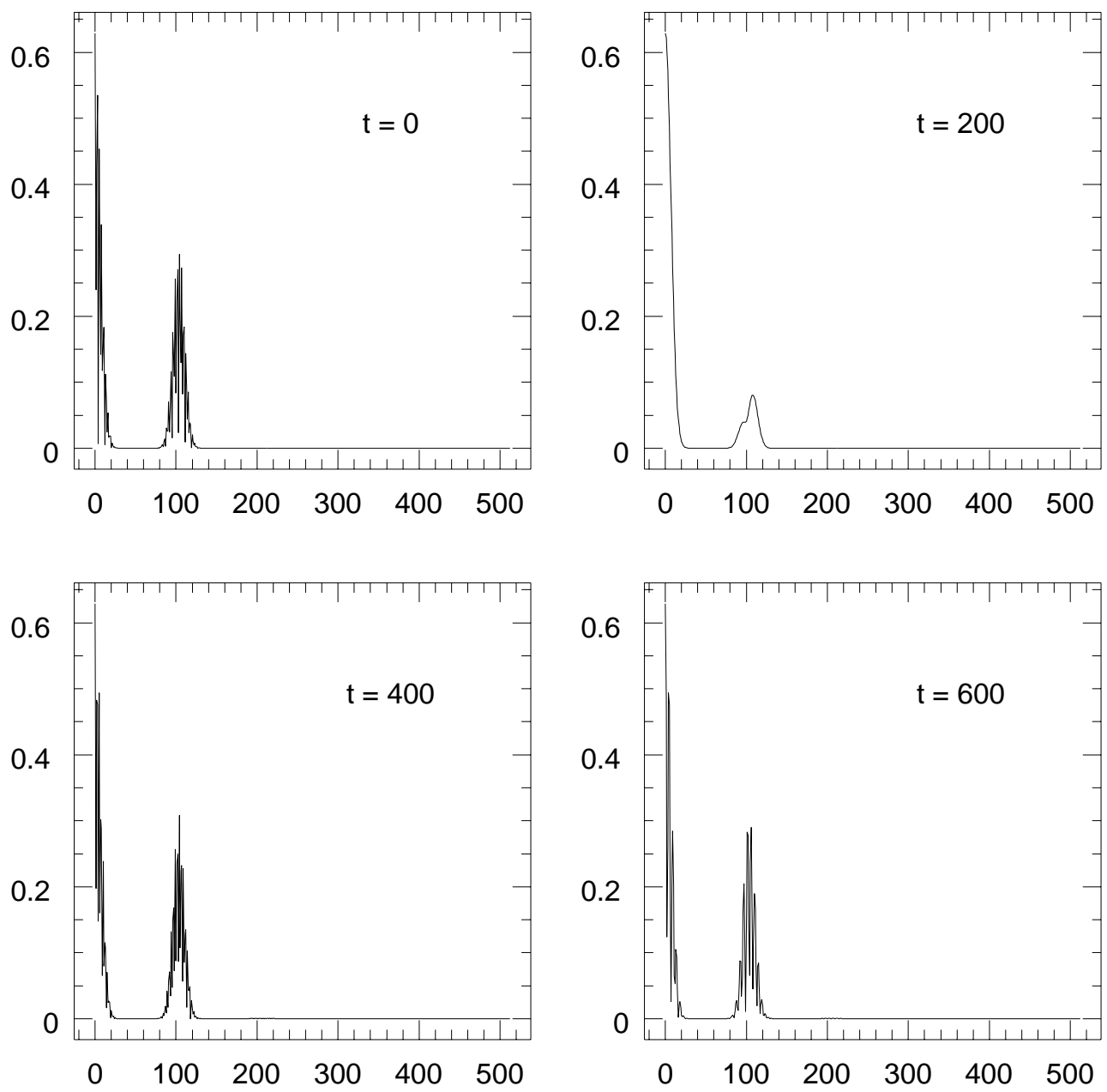


Fig.3

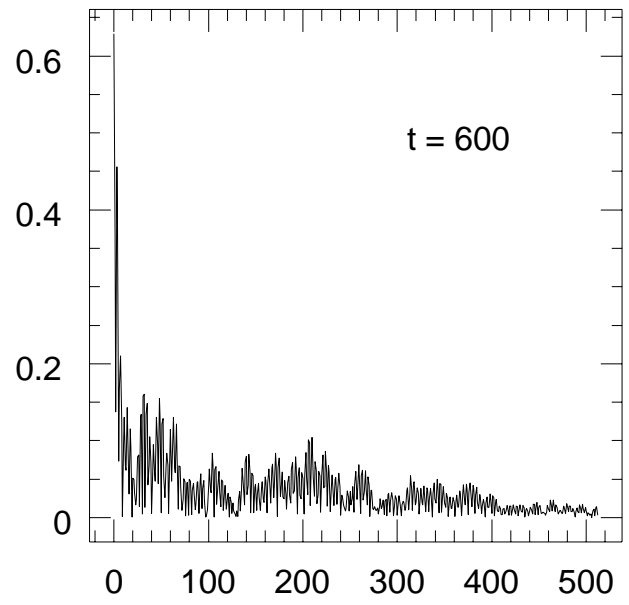
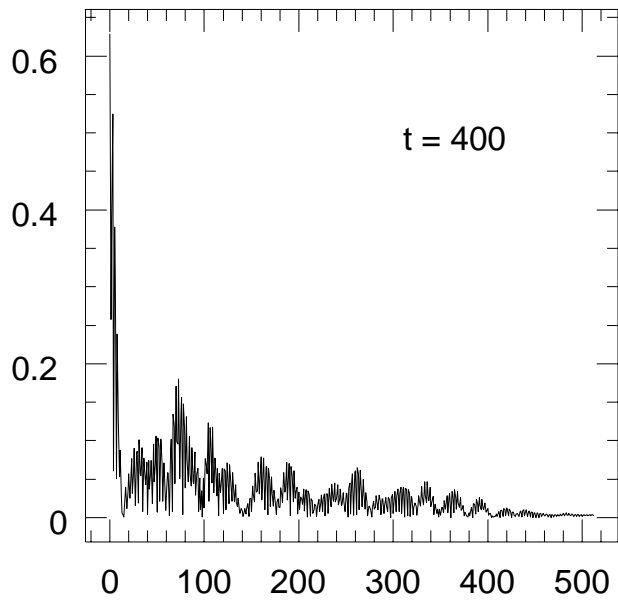
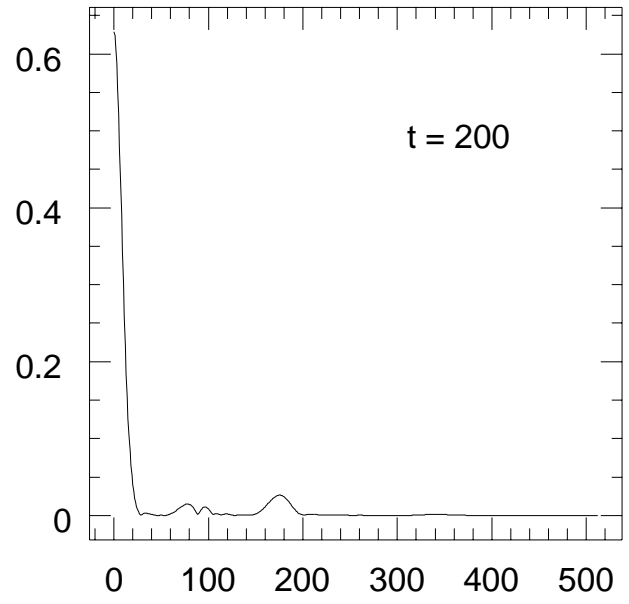
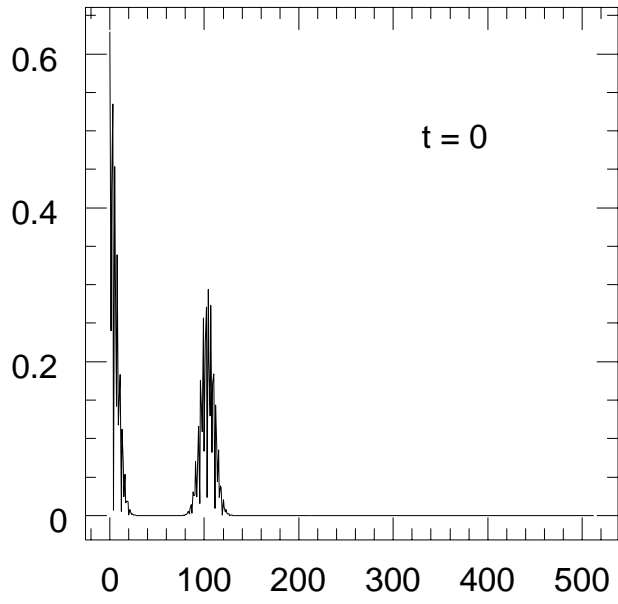


Fig.4



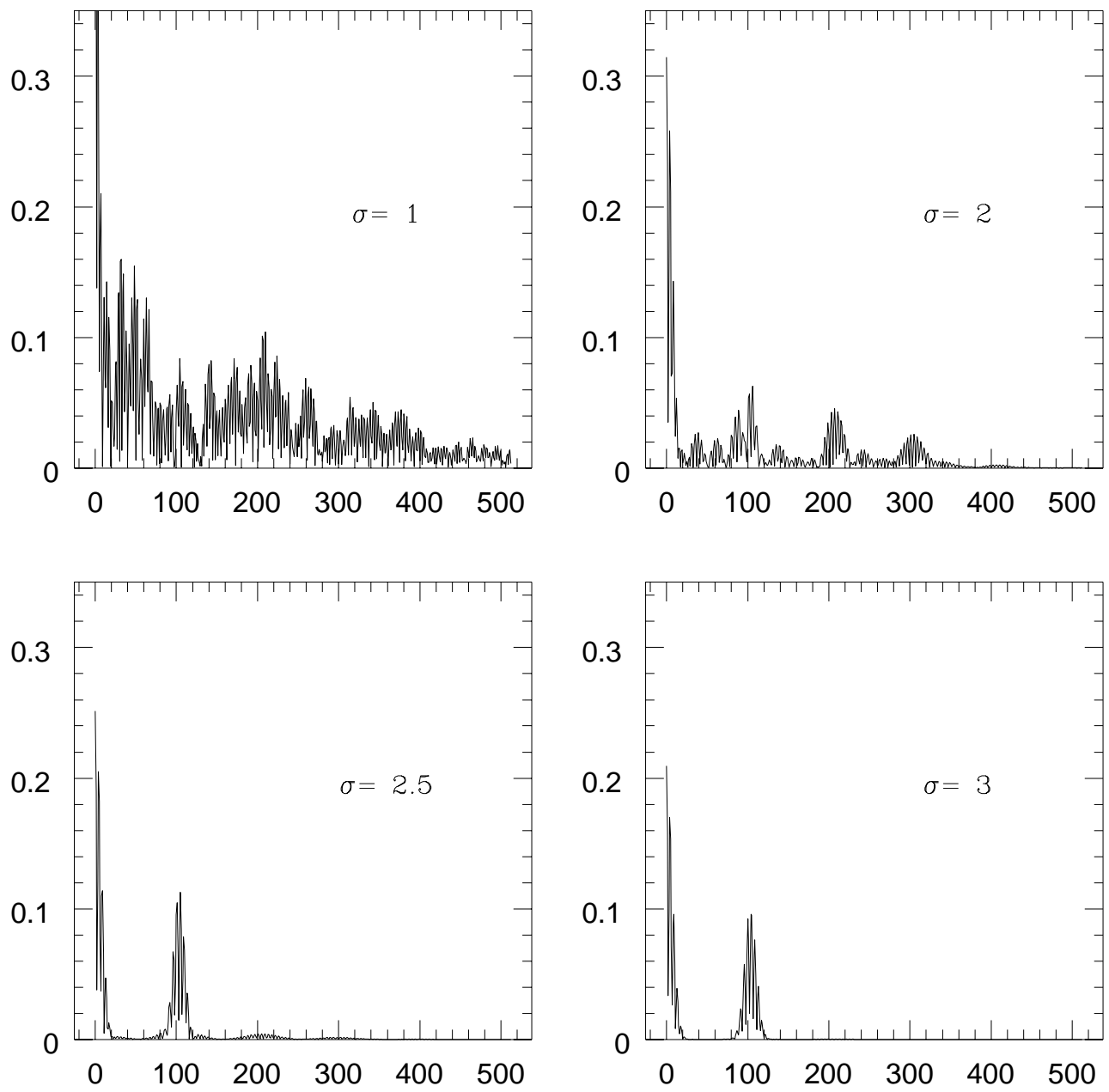


Fig.5

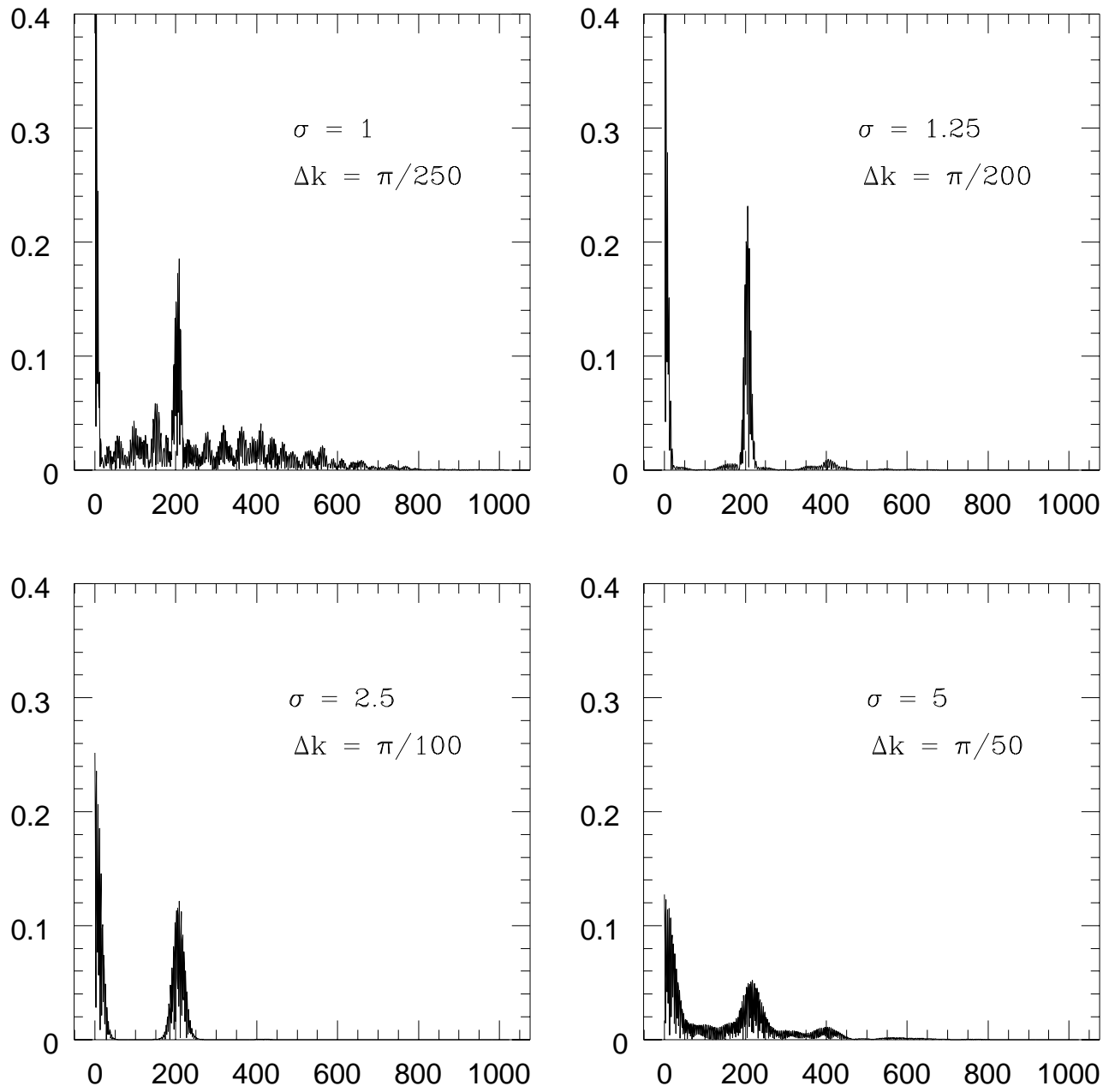


Fig.6

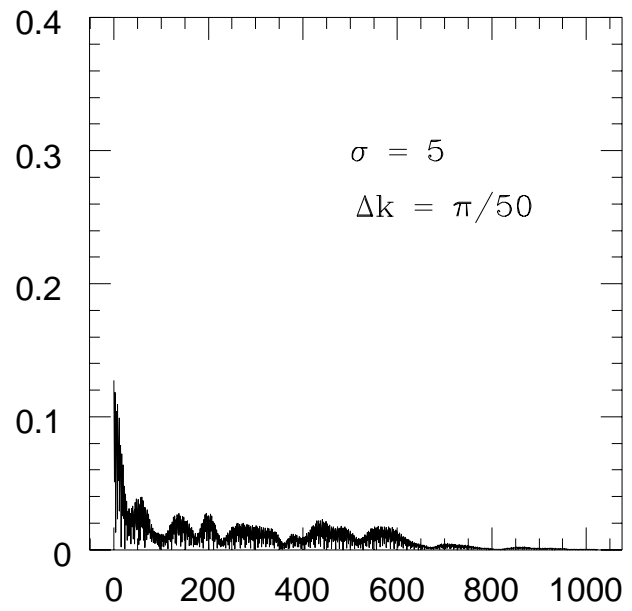
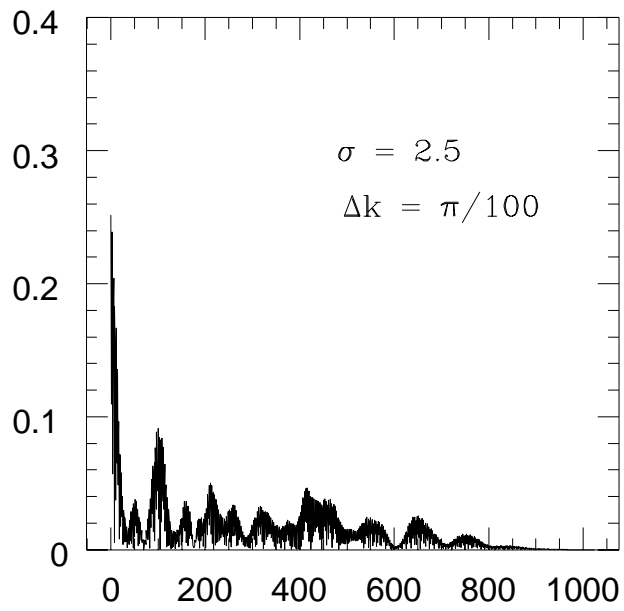
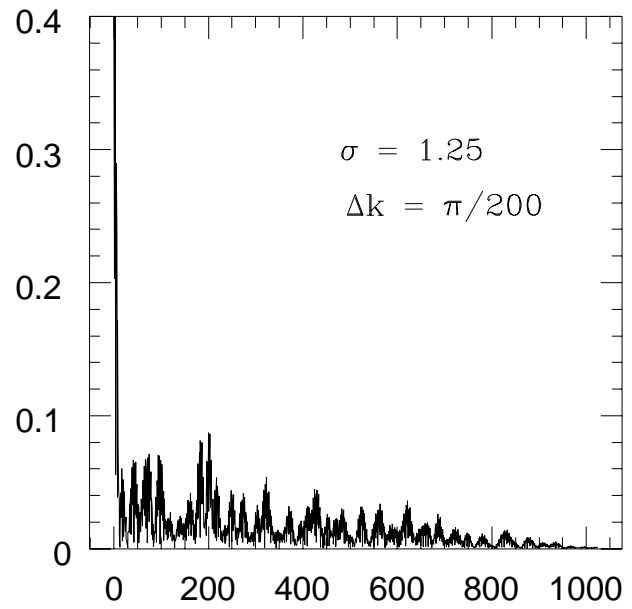
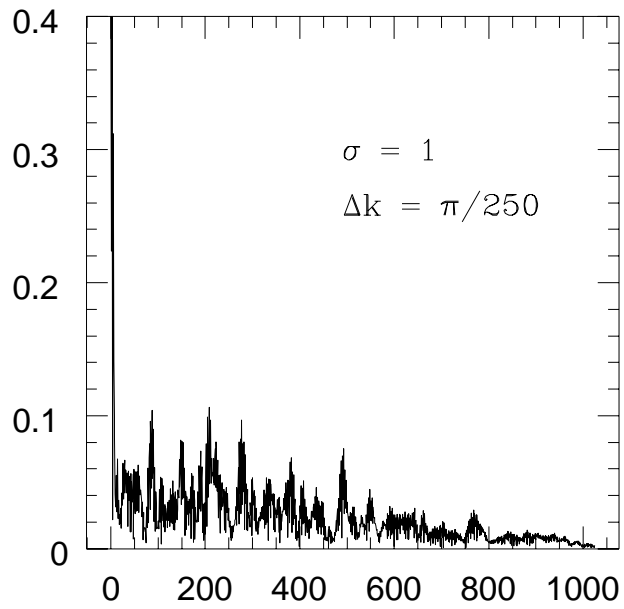


Fig.7

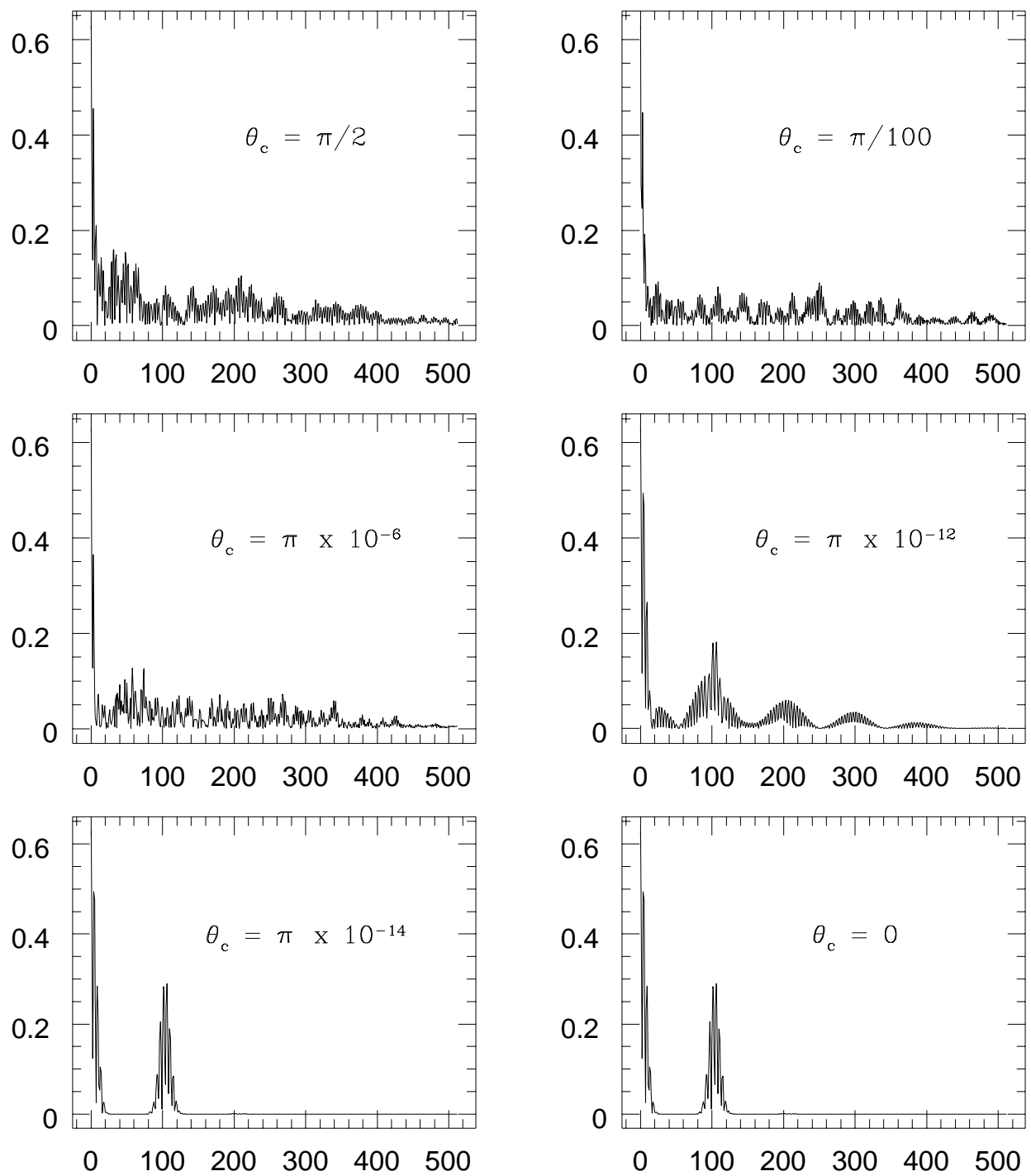


Fig.8

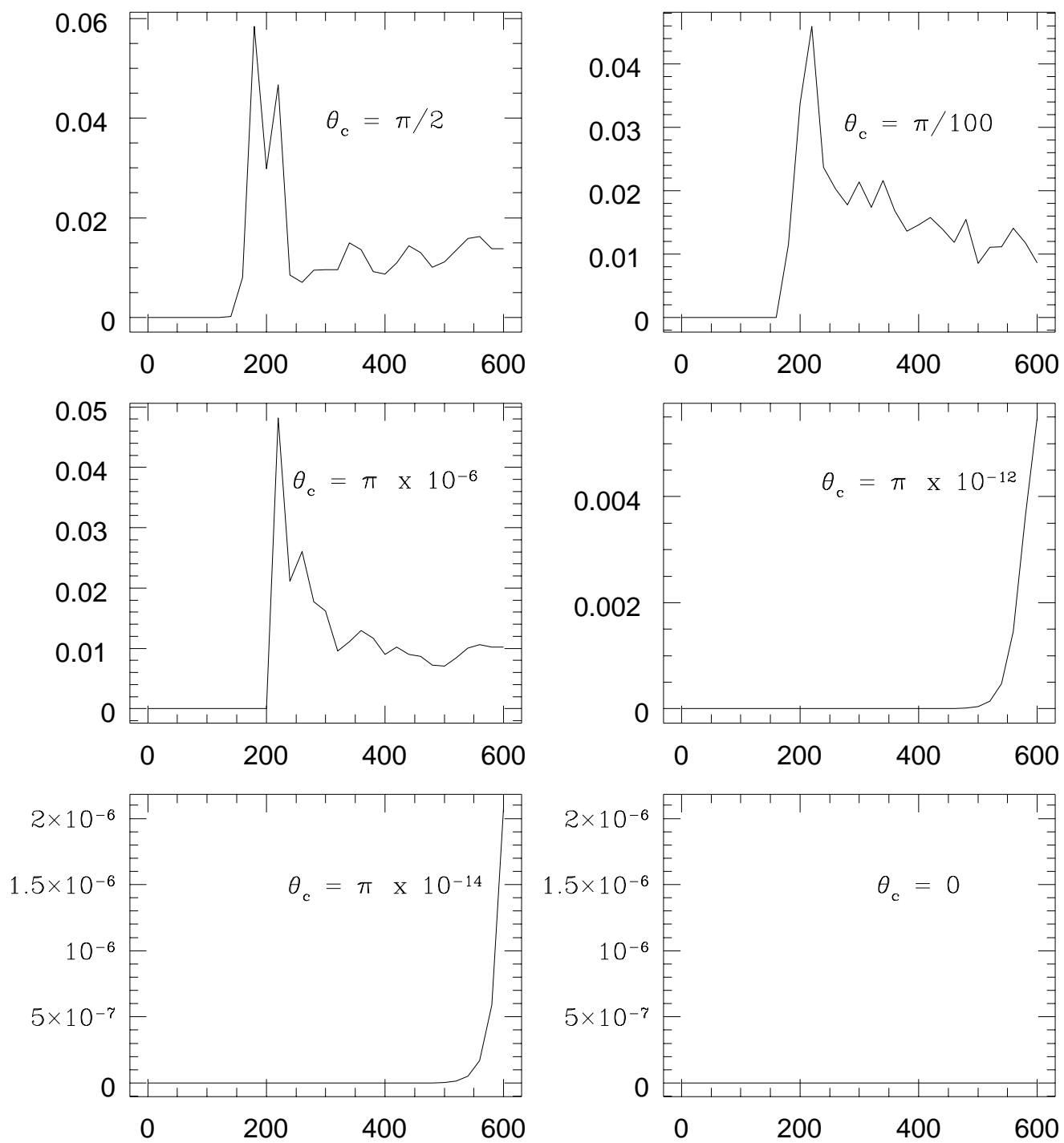


Fig.9

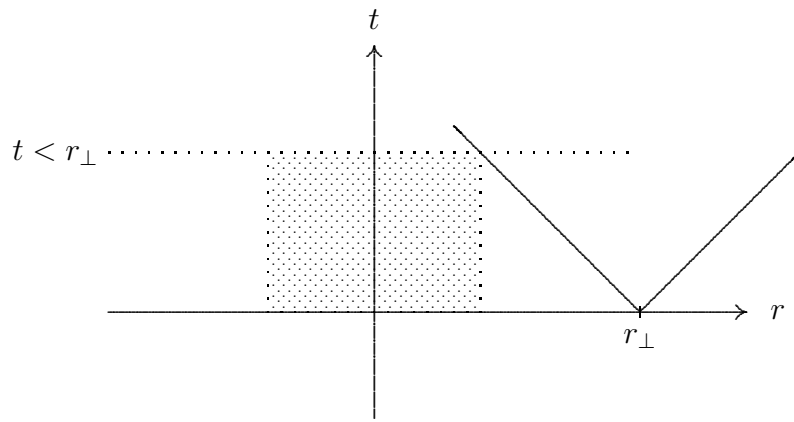


Fig.10

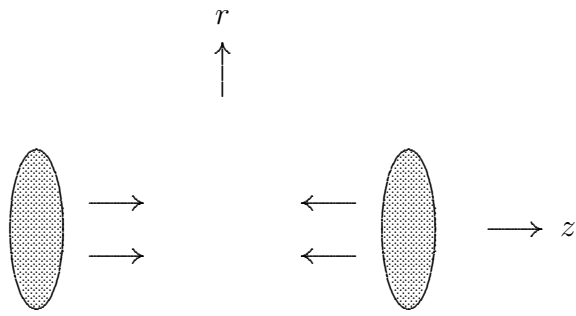


Fig.11